

I-V Characteristics of Polycrystalline CAZTSe Heterojunction Solar Cells at Different Ag Content and Annealing Temperatures

H. I. MOHAMMED¹, Ghuzlan Sarhan Ahmed², Seham hassan Salman³, Israa Akram Abbas⁴ and Sarah M. Obaid^{5,*}

^{1,2,3}Department of Physics, College of Education for Pure Science (Ibn-Alhaitham),
University of Baghdad, Baghdad, Iraq.

²Department of Physics, College of Education for Pure Science, Al-Mustansiriyah University, Iraq

³ Biomedical Engineering Department, Al-Mustaqbal University College

Received 3 November 2022, Revised 17 December 2022, Accepted 18 January 2023

ABSTRACT

Since CAZTSe demonstrated good optical absorption performance in the visible region, the focus of the present study is to grow the polycrystalline $(Cu_{1-x}Ag_x)_2ZnSnSe_4$ thin films deposited by thermal evaporation method on silicon substrates with 800nm thickness and 0.53nm/sec deposition rate as a function of Ag content (0.0,0.1,0.2) and annealing temperature at 373 K, 473 K. From I-V measurements of Al/n-CdS/p-CAZTSe/n-Si(111)/Al heterojunction solar cells under dark and illumination conditions, we observed that the forward bias current changes roughly exponentially with bias voltage and the ideality factor and saturation current dependence on both x content and Ta

Keywords: Polycrystalline CAZTSe, Ag content and annealing temperature, I-V characteristics

1. INTRODUCTION

In the past decades, two thin film technologies based on CdTe and CuInGaSe₂ (CIGS) have appeared [1,2]. These devices have achieved conversion efficiency exceed 20% [3,4]. Although this type of cells has reached the commercial producing stage [5], the scarcity and cost of Te and In, in addition to the toxicity of Cd [6,7] have limited their widespread utilize [8]. Therefore, researchers have focused on finding alternate absorber layers made of available and non-toxic materials [2,9]. So, they substituting the rare earth indium (In) and gallium (Ga) in CIGS compound with zinc (Zn) and tin (Sn) with appropriate stoichiometry to get copper zinc tin sulphide (CZTS) or selenide (CZTSe) [10]. Cu₂ZnSnSe₄ has drawn important interest due to its coefficient of high absorption, p-type conductivity, suitable direct band gap as well as, earth-abundant and nontoxic component elements [11,12]. Although CZTSe based solar cells have achieved high photoconversion efficiency, they remain lag behind the commercial solar cells because of the limited open circuit voltage (V_{oc}) [13]. To deal with this issue, the density of acceptors CuZn antisite defects must be reduced by replacing Cu with element of bigger size. Although Ag is considered not earth-abundant element, it is an important nominee to replace Cu because it is atomic radius about 16% larger and it belongs to the same chemical group [14]. The original material's band gap will be altered by this process, but the crystal structure and cation coordination will remain unchanged [15]. Henry *et al.* [16] analyzed the properties of vacuum-evaporated Cu₂ZnSnS₄ (CZTSe), CuAgZnSnS₄ (CAZTSe), and Ag₂ZnSnS₄ (AZTSe) thin films. They confirmed shown a peak shift toward the lower angle for CAZTSe and AZTSe films in the presence of tetragonal-structured CZTSe. Higher mobility was shown by the CAZTSe film, which is advantageous for solar applications. Sa and Liu [17] investigated theoretically the structural, mechanical, electronic, and optical properties of $(Cu_{1-x}Ag_x)_2SnZnSe_4$ (CAZTSe) solid solutions. From their study they confirm the mechanical stability for each compound. Thin film solar cells

Note: Accepted manuscripts are articles that have been peer-reviewed and accepted for publication by the Editorial Board. These articles have not yet been copyedited and/or formatted in the journal house style.

made of CuAgZnSnSe₄ (CAZTSe) were created on a variety of conducting substrates (Al, Cu, Ag, FTO, and AZO). Initial vacuum evaporation fabrication of non-commercial conducting substrates (Al, Cu, and Ag) by Henry *et al.* [18], then, using the vacuum evaporation technique, CAZTSe thin films were formed on both commercial and non-commercial conducting substrates (FTO and AZO). The CAZTSe films' band gap ranged from 1.514 to 1.893 eV. All of the films had n-type conductivity, according to Mott-Schottky plots, and the carrier concentration was in the 10¹⁸–10¹⁹ cm⁻³ range. Mora-Herrera and Pal [19] argued that a tandem solar cell made of monolithic kesterite that can absorb light across a broad spectral range. Cu₂ZnSnS₄ (CZTS) top cell with a greater band gap and an underlying (Ag_xCu_{1-x})₂ZnSnSe₄ (ACZTSe) bottom cell with a smaller band gap make up the suggested tandem structure. They are coupled in a series circuit via a tunneling junction.

The goal of the present study is to deposit polycrystalline (Cu_{1-x}Ag_x)₂ZnSnSe₄ thin films on silicon substrates with 800nm thickness and 0.53nm/sec deposition rate as a function of Ag content (0.0,0.1,0.2) and annealing temperature (373, 473) K using the thermal evaporation technique. The I-V characteristics of the prepared films will be measured and discussed.

2. Experimental Procedure

The CAZTSe HJs solar cells fabricated, the single crystal silicon wafer substrates were used. These substrates were carefully cleaned by using several methods depend on the type of substrate. Thin layer of Al was deposited on the anti-reflected face of Si wafer as back electrode for HJs. The required amount of (Cu_{1-x}Ag_x)₂ZnSnSe₄ powder which depends on the value of x to achieve the desired thickness of 800nm had been located into a molybdenum boat which tied in the vacuum chamber between two electrodes. When the system was pumped down to 10⁻⁵ Torr, the Si/Al substrates were fixed to the substrates holder and positioned at a height of 18 cm above the boat, when the boat reached the required temperature, the deposition process began with a 0.53 nm/sec deposition rate after an electric current was gradually passed through it. After all the material evaporated, the current was gradually reduced to zero. The same steps were used to deposit thin CdS films with 100 nm and 0.3 nm/sec deposition rate on CAZTSe/Si/Al structures using CdS powder which provided from (Balzers) Company with a high purity of 99.999%. The deposited films were left under high vacuum for one day. Some of prepared samples were annealed at temperatures of 373 K and 473 K under vacuum for 1h using electrical furnace. The last step to complete the fabrication of the HJ solar cells, suitable electrodes were deposited on the CdS/CAZTSe/Si/Al structures of Al metal using a suitable mask.

A 70 nm CdS buffer layer, deposited via chemical bath, completes the solar cells. The samples are submerged in a solution containing ammonium acetate (20 mM), thiourea (5.1 mM), cadmium acetate (1 mM), and ammonia (0.3 mM) for 15 minutes while being agitated at 600 rpm. In an MRC2 chamber, the 50 nm/250 nm i-ZnO/ZnO:Al (Al₂O₃ 2 at%) window layer is RF-sputtered without purposeful sample heating. Thermal evaporation is used to create Ni (50 nm) and Al (500 nm) grids on top of the solar cell. Each sample has at least ten hands inscribed 0.5 x 0.5 cm² solar cells.

Finally, the front and back Al electrodes were connected to appropriate wires for carrying out the electrical measurements of the cell. I-V measurements of light, open circuit voltage (V_{oc}), short circuit current (I_{sc}), maximum power point (P_m), fill factor (F.F.), and photovoltaic conversion efficiency (PCE, η) were estimated for solar cells. The Fill factor and photovoltaic conversion efficiency were estimated using standard equations [20, 21]:

$$F. F. = \frac{P_{\max}}{V_{oc}I_{sc}} = \frac{V_{\max} I_{\max}}{V_{oc}I_{sc}} \quad (1)$$

$$\eta = \frac{P_{\max}}{P_{\text{in}}} * 100\% = \frac{\text{F.F.} \cdot V_{\text{oc}} \cdot I_{\text{sc}}}{P_{\text{in}}} * 100\% \quad (2)$$

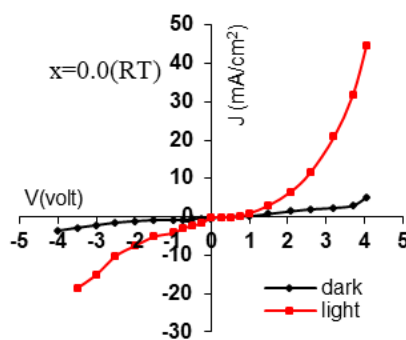
While, from dark Measurements in (I-V) the major diode parameters were evaluated, such as ideality factor (β) and saturation current (I_s). The ideality factor was obtained by using following relation [20]:

$$\beta = \frac{q}{k_B T} \left[\frac{V_f}{\ln(I_f/I_s)} \right] \quad (3)$$

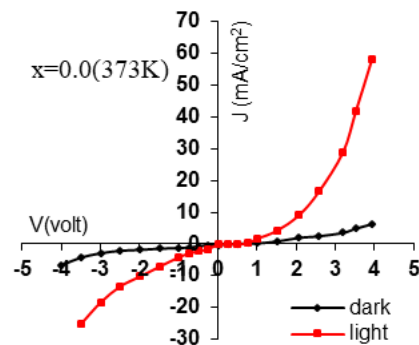
where q is the charge of an electron, T stands for the absolute temperature, k_B for the Boltzmann constant, and V_f for the forward bias voltage., and I_f denotes the forward bias current. Black box and Halogen lamp light of ($40\text{mW}/\text{cm}^2$) power density (P_{in}) was used to obtain dark and light (I-V) measurements, respectively under forward and reverse bias.

3. RESULTS AND DISCUSSION

One of the crucial characteristics of the junction is the current-voltage curve, which depicts how the resulting current behaves with applied forward and reverse bias voltage [21]. Figure 1 depicted the I-V characteristics curve of the prepared Al/CdS/(Cu $_{1-x}$ Ag $_x$) $_2$ ZnSnSe $_4$ /Si/Al HJ solar cells at RT with various Ag content of 0 (panels a, b,c), 0.1 (panels d, e, f), and 0.2 (panels g, h, i) and annealing temperatures (373 and 473) K at forward and reverse bias voltage in the dark and illumination conditions. In general, the applied voltage injects majority carrier, which causes the forward dark current to be created, and this reduces the built-in potential as well as the depletion region's width [22]. Then, the majority and minority carrier concentrations are higher than the intrinsic carrier concentration, i.e $p_n > n_i^2$ leading to generate a recombination current in the low voltage region (0-0.3volt). However, the tunnelling current is resented in the region of high voltage (0.3V). Following that, the current value rapidly increases exponentially as the voltage increases, and this is known as the diffusion current [23, 24]. The reverse bias current includes two regions. The first region is the generation current, which depends on the bias voltage. The width of the depletion region and the generation current both increase as the bias voltage rises. The reverse bias current stabilizes and becomes independent of the bias voltage in the diffusion current, the second region [25]. It can be seen from Figure 1 that the behaviour of the current under illumination at forward and reverse bias voltage is similar to that of the dark current with an apparent increase in the current value. During the cell illumination, CAZTSe Photons with energies equal to or greater than the CAZTSe band gap energy are absorbed by semiconductors, this creates e-h pairs in the depletion region which are separately driven at the interface by the electric field [26]. Another observation from the same figure is that the illumination current increases when x content and T_a increase due to the improvement in the film depletion region width, film absorbance, carrier mobility, and film crystal structure with increasing x value and T_a .



(a)



(b)

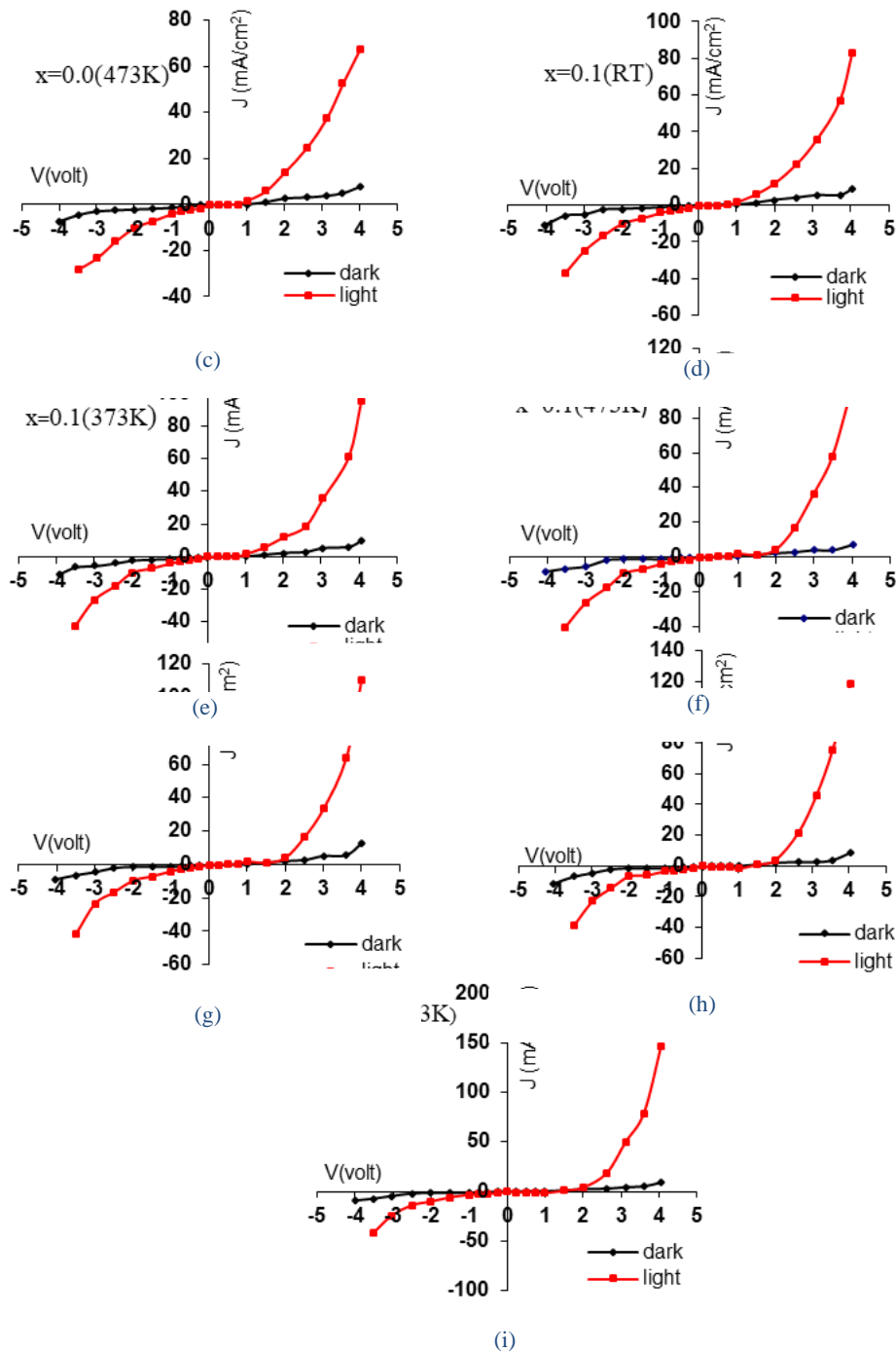
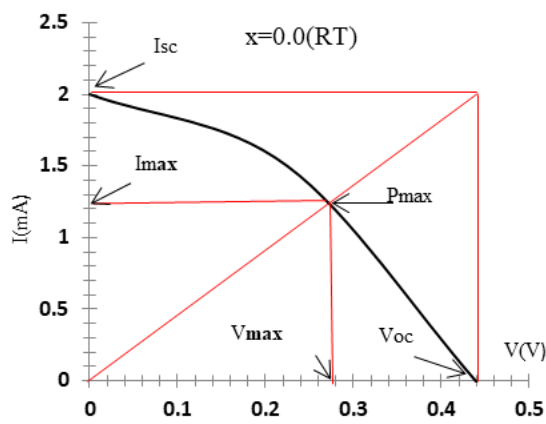


Figure1: J-V characteristics under dark and illumination for Al/CdS/(Cu_{1-x}Ag_x)₂ZnSnSe₄/Si/Al HJ solar cells with various x content and Ta.

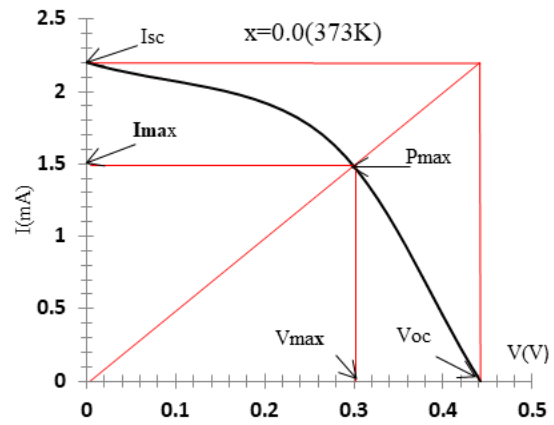
The parameters open circuit voltage (V_{oc}) and short circuit current (I_{sc}) are essential because they can identify the region in which the heterojunction operates. The magnitude of V_m (maximum voltage) and I_m (maximum current) are estimated at maximum power point on the photovoltaic power output curve as seen in Figure 2 with Ag content for 0 (panels a, b,c), 0.1 (panels d, e, f), and 0.2 (panels g, h, i). The fill factor and efficiency, calculated by using Eqs. (1)

Note: Accepted manuscripts are articles that have been peer-reviewed and accepted for publication by the Editorial Board. These articles have not yet been copyedited and/or formatted in the journal house style.

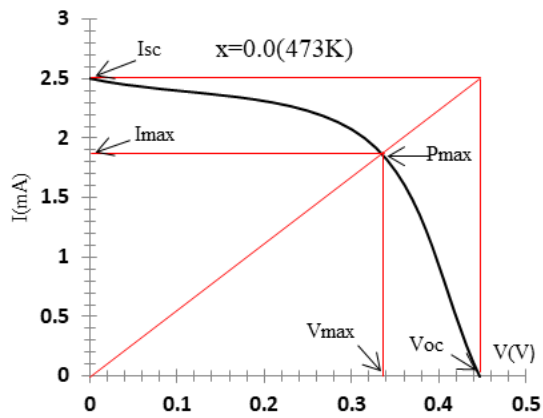
and (2), respectively. The results are summarized in Table 1. Table shows that the values of V_{oc} and I_{sc} are increased as x value and T_a increased which in turn increase the V_{max} , I_{max} and the F.F. This may be attributed to the improvement in the absorber layer properties with increasing x content and T_a . It is also noticed that the photoconversion efficiency (PCE) of the cell increases with increasing x content and T_a . This may be due to increase the particle size of the absorber layer with increasing Ag content and T_a . Because the minority carrier diffusion length and built-in potential are both maximized by large particle size in the absorber layer, the PCE of the constructed cell is significantly correlated with particle size [27, 28]. The rise in PCE can also be related to the expansion of the depletion region [29, 30]



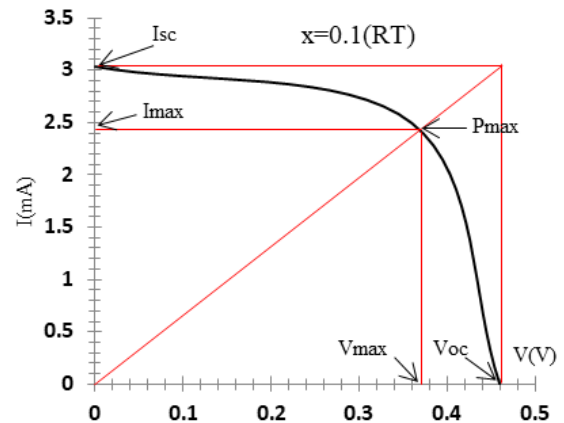
(a)



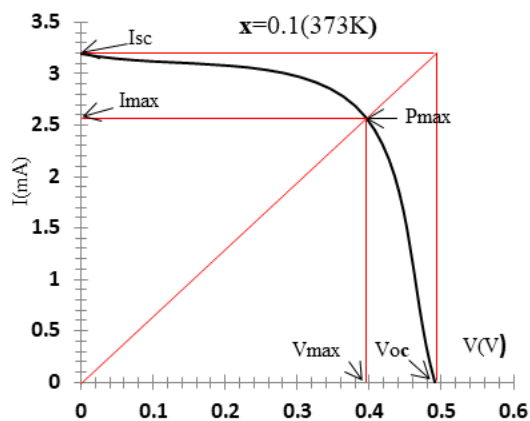
(b)



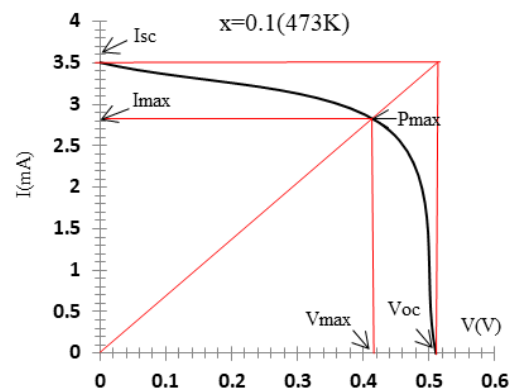
(c)



(d)



(e)



(f)

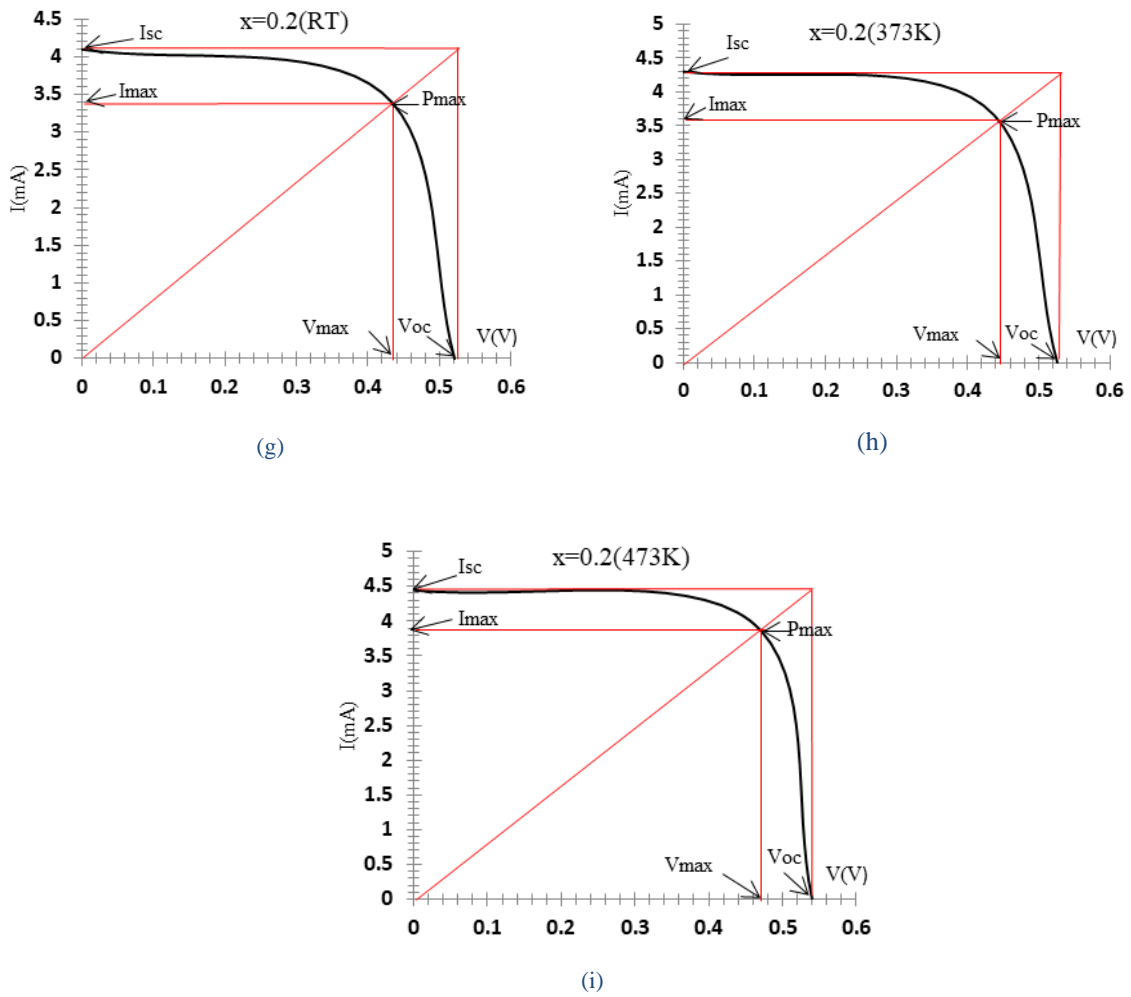
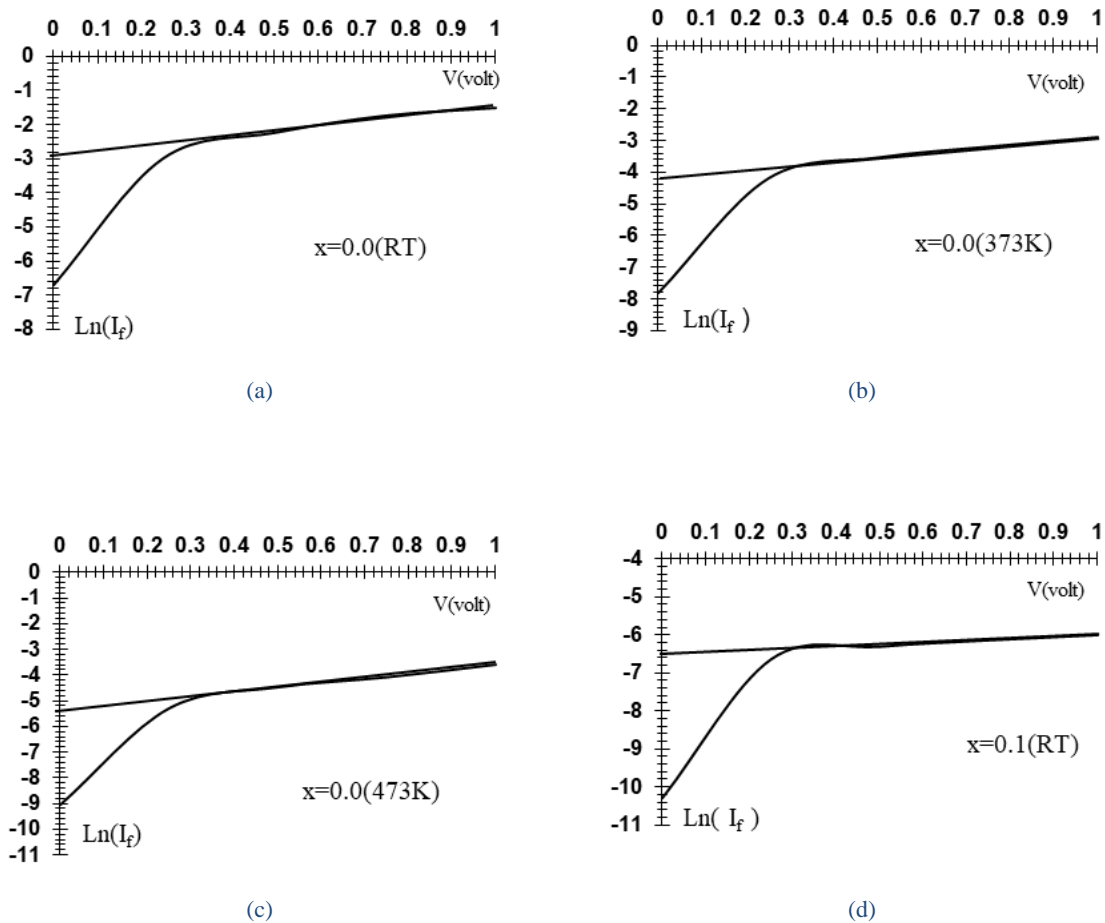


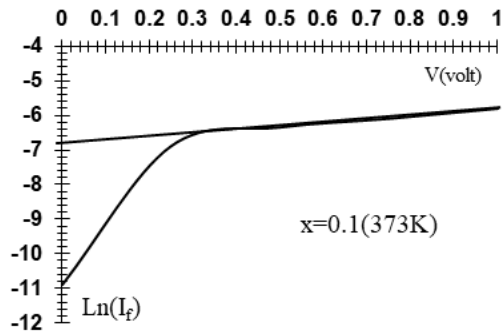
Figure2: I_{sc} and V_{oc} curves for Al/CdS /CAZTSe/Si/Al HJs solar cells with various x value and T_a

Table 1. The values of I_{sc} , V_{oc} , I_{max} , V_{max} , F.F and efficiency (η %) for Al/CdS/(Cu $_{1-x}$ Ag $_x$) $_2$ ZnSnSe $_4$ /Si/Al HJs solar cells with various x value and T_a .

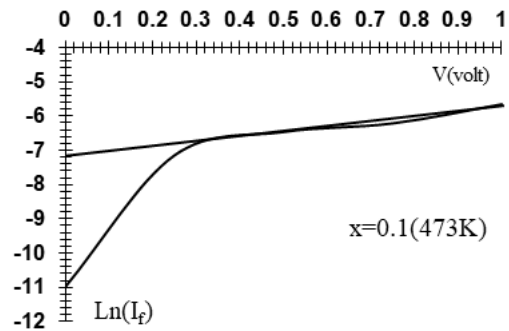
x	T_a (K)	I_{sc} (mA)	V_{oc} (V)	I_{max} (mA)	V_{max} (V)	F.F.	η %
0	RT	2	0.44	1.23	0.275	0.3844	0.529
	373	2.2	0.442	1.5	0.31	0.4782	0.727
	473	2.5	0.447	1.87	0.335	0.5606	0.979
0.1	RT	3.04	0.46	2.43	0.37	0.6429	1.405
	373	3.2	0.49	2.56	0.398	0.6498	1.592
	473	3.5	0.51	2.82	0.413	0.6525	1.82
0.2	RT	4.1	0.52	3.38	0.433	0.6865	2.287
	373	4.3	0.527	3.6	0.442	0.7022	2.486
	473	4.44	0.54	3.85	0.47	0.7547	2.827

Figure 3 shows the relations between the forward dark current logarithm as a function of applied voltage (0-1) V for prepared Al/CdS/(Cu_{1-x}Ag_x)₂ZnSnSe₄/Si/Al photovoltaic cells at RT with various with Ag content for 0 (panels a, b,c), 0.1 (panels d, e, f), and 0.2 (panels g, h, i) and annealing temperatures 373K and 473K. This Figure shows that the forward current consists of two regions. The first region represents the recombination current due to increase the carrier at low bias, while the second region represents the tunnelling current due to decrease the width of the depletion region with increasing the bias voltage resulting in increasing the chance of carrier tunnelling. From the first region, the ideality factor (β) of the prepared HJs was calculated using Eq. (3) and the obtained results are listed in Table (2). The physical meaning of the ideality factor being greater than (2) is that the tunnelling plays a significant role with the recombination-emission [31]. The value of the diode ideality factor is a key aspect for diagnosing the type of the recombination and its location within the device [32]. As shown in Table (2), the value of the ideality factor is greater than unity ($\beta > 1$) which means that the dark current results from the non-ideal recombination of electrons and holes in the space charge region. The reverse saturation current (I_s) for all samples is determined from the intercept of the straight line with the current axis at zero bias voltage as seen in Figure (3), and the obtained data are listed in Table (2). The Decreased values of β and I_s with increasing x content and T_a indicates the improvement in the crystal structure and the reduction of the defects that act as active recombination centres, resulting in lower recombination rates for the e-h pairs and improved solar cell performance.

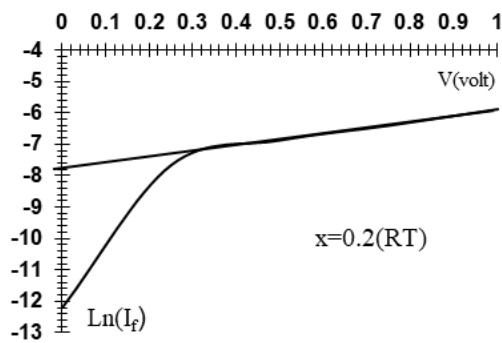




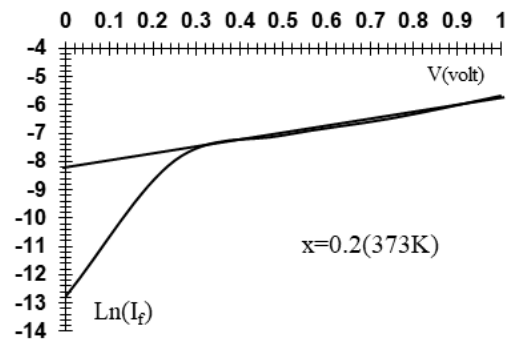
(e)



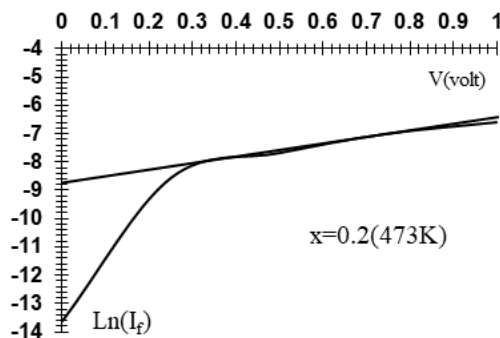
(f)



(g)



(h)



(i)

Figure3: $\ln(I)$ as a function of V for dark forward bias for $\text{Al}/\text{CdS}/(\text{Cu}_{1-x}\text{Ag}_x)_2\text{ZnSnSe}_4/\text{Si}/\text{Al}$ HJs solar cells with various x value and T_a .

Table 2: Values of ideality factor and saturation current for CdS/CAZTSe/Si HJs solar cells for different x content and Ta.

x	Ta(K)	Ideality factor (β)	Saturation current (I_s) mA
0	RT	3.0351	0.055
	373	3.0059	0.015
	473	2.9566	0.0045
0.1	RT	2.8402	0.0015
	373	2.7969	0.00011
	473	2.7459	0.00074
0.2	RT	2.5472	0.00041
	373	2.4686	0.00027
	473	2.3993	0.00015

4. CONCLUSION

In this study, I-V characteristics under illumination showed that the performance of the manufactured solar cell improved with increasing x value and Ta. Therefore, the optimum conditions in which the cell will operate for best performance ($F.F=0.7547$ and $\eta=2.827\%$) are when x value and Ta equal to 0.2 and 473K, respectively. I-V measurements under dark with forward bias for all prepared Al/CdS/CAZTSe/Si/Al HJs showed that the values of the demonstrated that as x content and Ta increased, the values of the ideality factor and saturation current decreased.

REFERENCES

- [1] Guo, H., Ma, C., Zhang, K., Jia, X., Li, Y., Yuan, N., & Ding, J., Solar Energy Materials and Solar Cells, vol **178**, (2018) pp.146-153.
- [2] Green, M.A., Progress in Energy, vol **1**(1) (2019) p.013001.
- [3] Friedlmeier, T.M., Jackson, P., Bauer, A., Hariskos, D., Kiowski, O., Menner, R., Wuerz, R. and Powalla, M., Thin Solid Films, vol **633** (2017) pp.13-17.
- [4] Tina, G.M., Scavo, F.B., Merlo, L. and Bizzarri, F., Applied Energy, vol **281** (2021) p.116084.
- [5] Mansfield, L.M., Kanevce, A., Harvey, S.P., Bowers, K., Beall, C., Glynn, S. and Repins, I.L Progress in Photovoltaics: Research and Applications, vol **26**(11) (2018) pp.949-954.
- [6] Exarhos, S., Palmes, E., Xu, R. and Mangolini, L RSC advances, vol **7**(41) (2017) pp.25575-25581.
- [7] Lai, F. I., Yang, J. F., Wei, Y. L., & Kuo, S. Y., vol.**19**, issue 3(2017)795-802.
- [8] Fthenakis, V., Athias, C., Blumenthal, A., Kulur, A., Magliozzo, J., & Ng, D, Renewable and Sustainable Energy Reviews, vol. **123**, (2020) pp.109776.
- [9] Kuo, D. H., & Wu, H. P., Advanced Materials Research, vol. **463**, (2012). pp. 602-606.
- [10] Simya, O. K., Priyadarshini, B. G., Balachander, K., & Ashok, A. M., Materials Research Express, vol **7**, issue 1, (2020) pp. 016419.

- [11] Kim, J., Park, S., Ryu, S., Oh, J. and Shin, B., Progress in Photovoltaics: Research and Applications, vol. **25**(4) (2017) pp.308-317.
- [12] Wang, A., Chang, N.L., Sun, K., Xue, C., Egan, R.J., Li, J., Yan, C., Huang, J., Rong, H., Ramsden, C. and Hao, X., Sustainable Energy & Fuels, vol **5**(4) (2021) pp.1044-1058.
- [13] Gershon, T., Sardashti, K., Lee, Y. S., Gunawan, O., Singh, S., Bishop, D., & Haight, R., Acta Materialia, vol **126** (2017) pp. 383-388.
- [14] Goktas, A., Tumbul, A. and Aslan, F., Journal of Sol-Gel Science and Technology, vol **90**(3) (2019.) pp.487-497.
- [15] Mohammed. H. I., Ph.D. thesis, University of Baghdad (2021).
- [16] Henry, J., Sivakumar, G., Vettumperumal, R., Subramanian, T. and Mohanraj, K., Materials in Electronics, vol **32**(15) (2022) pp.20259-20272.
- [17] Sa, R. and Liu, D., Materials Chemistry and Physics, vol **279** (2022) p.125757.
- [18] Henry, J., Mohanraj, K. and Sivakumar, G., . Vacuum, vol 160 (2019) pp.347-354.
- [19] Mora-Herrera, D. and Pal, M., Physica E: Low-dimensional Systems and Nanostructures, vol. **138** (2022) p.115056.
- [20] Bayod-Rújula, A.A., Solar photovoltaics (PV). In Solar Hydrogen Production (pp. 237-295). Academic Press. (2019).
- [21] Siu, C., Semiconductor physics. In Electronic Devices, Circuits, and Applications (pp. 35-39). Springer, Cham. (2022).
- [22] Fdhala, M., Hemed, A., Al-Ansari, R., Al-Haddad, R. and Abbas, R., Kuwait Journal of Science, vol **49**(2) (2022).
- [23] Sze, S. M., & Ng, K. K., 3rd ed. John Wiley & Sons: Hoboken NJ, USA, (2007)134-196.
- [24] Kittel, C. and McEuen, P., Introduction to solid state physics. John Wiley & Sons, (2018).
- [25] Lee, M., Ryu, H.Y., Ko, E. and Ko, D.H., ACS Applied Electronic Materials, vol. **1**(3) (2019) pp.288-301.
- [26] Shelke, H. D., Lokhande, A. C., Patil, A. M., Kim, J. H., & Lokhande, C. D., Surfaces and Interfaces, vol **9**, (2017) pp. 238-244.
- [27] Henry J., Mohanraj K., Sivakumar G., Vacuum J., vol **156**, (2018) pp.172-180.
- [28] Henry, J., Mohanraj, K., & Sivakumar, G., Vacuum, vol **160** (2019) pp.347-354.
- [29] Henry J., Mohanraj K., Sivakumar G., J. Phys. Chem. C **123**, (2019) pp.2094.
- [30] Zhan, L., Ning, X., Zhou, X., Luo, J. and Fan, X., 2022. Advanced Powder Technology, vol. **33**(4) (2022) p.103521
- [31] Lee, J.H., Hiramoto, M. and Izawa, S. Japanese Journal of Applied Physics, vol. **61**(1) (2021) p.011001.
- [32] Courtier N. E., Phys. Rev. Applied, vol **14**, (2020) pp. 024031.
- [33] Meyer E. L, International Journal of Photoenergy, vol **2017**, (2017).